2003

The rotational spectrum of iodine dioxide, OIO

Charles E. Miller
Haverford College

Edward A. Cohen

The rotational spectrum of iodine dioxide, OIO

Charles E. Miller and Edward A. Cohen

Citation: J. Chem. Phys. **118**, 6309 (2003); doi: 10.1063/1.1540107
View online: http://dx.doi.org/10.1063/1.1540107
View Table of Contents: http://jcp.aip.org/resource/1/JCPSA6/v118/i14
Published by the American Institute of Physics.

The rotational spectrum of iodine dioxide, OIO

Charles E. Miller[a)]
Department of Chemistry, Haverford College, Haverford, Pennsylvania 19041-1392

Edward A. Cohen[b)]
Jet Propulsion Laboratory, California Institute of Technology, Pasadena, California 91109-8099

(Received 30 September 2002; accepted 3 December 2002)

The rotational spectrum of the OIO radical has been observed for the first time. Spectra of both the ground and first two excited bending vibrational states have been analyzed. Rotational, centrifugal distortion, fine, and hyperfine constants have been derived. These constants have been used to determine the molecular structure, harmonic force field, and electron distribution. The OIO molecular parameters are compared with those of OClO and OBrO. © *2003 American Institute of Physics.* [DOI: 10.1063/1.1540107]

INTRODUCTION

Iodine oxides have been known for more than 100 years, yet their chemical and physical properties remain poorly characterized. For more than 70 years only IO, the prototypical iodine oxide, had been identified in the gas phase.[1] Studier and Huston[2] first reported the detection of gas phase IO_2 which they observed in the thermal decomposition of I_2O_5. Gilles, Polak and Lineberger[3] obtained negative ion photoelectron spectra of IO_2^- that they assigned to $OIO(^2B_1) \leftarrow OIO^-(^1A_1)$ transitions based on the vibrational frequency arguments. However, it was not until the work of Himmelmann *et al.*[4] on the IO self-reaction that the existence of gas phase OIO was widely acknowledged. Himmelmann *et al.*[4] observed a strong, structured vibronic spectrum spanning the 400–700 nm range and deduced that the carrier was OIO based on similarities between the new spectrum and the electronic spectra of OClO[5] and OBrO.[6] Subsequent studies have shown that OIO is the principal product of the IO+BrO reaction,[7] that OIO is remarkably stable with respect to photodissociation in the visible,[8] and that OIO may serve as the starting point for the formation of iodine aerosols in the marine boundary layer.[9,10]

Little additional spectroscopic or structural information exists for OIO. Atherton *et al.*[11] observed electron paramagnetic resonance (EPR) spectra of OIO in KIO_2F_2 crystals, determining the g factor as well as the hyperfine and ^{127}I quadrupole coupling constants. Byberg[12,13] observed OIO in $KClO_4$ crystals for normal and $^{16}OI^{17}O$ and derived electronic charge and spin distributions that were very similar to those found for OClO and OBrO.[14] Maier and Bothur[15] observed infrared (IR) and electronic spectra of OIO isolated in Ar and O_2 matrices. Most recently, Misra and Marshall[16] calculated an OIO structure at the MP2=FC/6-311+G(3*df*) level of theory.

This paper reports the rotational spectrum and structural determination of OIO. The rotational spectrum of OClO has been well studied[17–20] and we have recently reported an analysis of the OBrO spectrum.[21] The OIO spectrum was discovered while searching for rotational transitions of highly excited vibrational levels of the IO $X_1\,^2\Pi_{3/2}$ state.[22] Subsequently, six-line hyperfine splitting patterns were observed which had strong Zeeman effect. These were clear indications of an iodine containing radical. It was assumed that the radical was OIO and extensive searches were conducted for more transitions. Eventually we assigned a sufficient number of transitions to provide an extensive analysis of the ground and $\nu_2=1$ states. After the experiments were completed, a smaller number of previously unassigned transitions were assigned for the $\nu_2=2$ state and some parameters were determined for that state as well. The following sections describe the experimental procedures for generating OIO, the assignment and analysis of the spectrum, and the interpretation of the spectral parameters in terms of molecular properties. These results are compared to those of the related molecules OClO and OBrO.

EXPERIMENT

The experimental procedures were initially identical to those recently described by Miller and Cohen[22] for the generation of IO. OIO was discovered during the measurement of highly excited vibrational states of IO using an external microwave discharge through O_2 and passing the products over solid I_2 held in a $18\times3.5\times2$ cm deep boat within the sample cell. The first feature observed which suggested the presence of secondary products is shown in Fig. 1. It is the strong $N_{K_aK_c},J,F=26_{2,25},26.5,29\leftarrow25_{1,24},25.5,28$ transition at the left of the scan. Two smaller features later identified as the $v_2=1$, $8_{8,1}$, 8.5,11$\leftarrow7_{7,0}$, 7.5,10, and $8_{8,1}$,8.5,10 $\leftarrow7_{7,0}$,7.5,9 transitions lie within the IO $v=11$ hyperfine pattern. Possibly because of changing conditions due to deposits of iodine and its oxides on the cell walls, production of OIO using an external oxygen discharge deteriorated severely. OIO production was considerably enhanced by passing a DC discharge through O_2 flowing over a container of I_2 as described in Ref. 22. I_2 was placed in a long necked glass bulb at the bottom of a 1 m by 7.3 cm i.d. double pass ab-

a)Electronic mail: cmiller@haverford.edu; http://www.haverford.edu/chem/miller/miller.html
b)Electronic mail: edward.a.cohen@jpl.nasa.gov; http://spec.jpl.nasa.gov

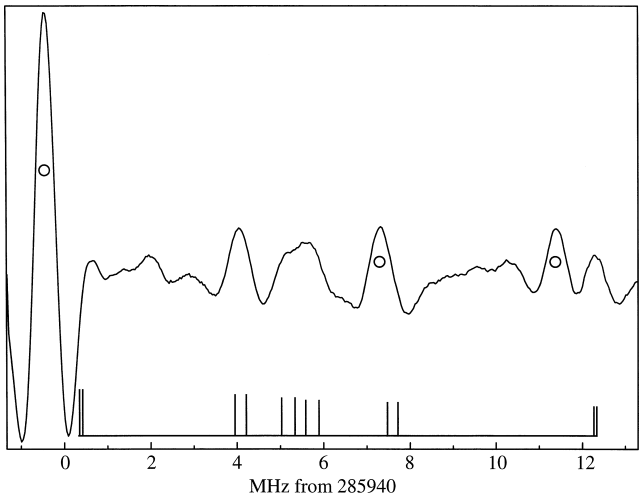

FIG. 1. The first feature (left) thought to indicate the presence of secondary products in the synthesis of IO. The calculated IO $v=11$ positions are shown by the stick spectrum. OIO features are indicated by circles. The baseline has been removed. See text for details.

sorption cell. O_2 was passed through the cell at ~25 l/s at pressures of 10 Pa. A DC discharge of ~35 ma at 1.3 kV was passed through the mixture. The cathode was a thin strip of 7.6 cm wide stainless steel shim stock which conformed to the inside diameter of the sample cell at one end while a grounded metal bellows valve in the sidearm to the pump served as the anode at the other end. A schematic view of the inlet region of the cell is shown in Fig. 2. A suitably strong feature for tuning the chemistry was chosen as the flow rate was throttled back while keeping the total pressure nearly constant until a maximum signal was attained. The exact flow rate was then not known, but it was estimated at ~4–6 l/s. The cell was maintained near room temperature by circulating methanol through an outer jacket. The conditions were difficult to maintain and reproduce due to copious solid deposits on the walls, electrodes and windows. Nevertheless, the strongest features were observable in survey scans with S/N of ≈40 for dwell times of 200 ms/point and ≈100 kHz steps. All spectra were recorded using tone burst frequency modulation[23] which produces a second derivative line shape. In order to confirm that the initially observed features were due to radical species, a constant magnetic field was applied with a Zeeman coil wound around the sample cell. Later assignments relied primarily on comparisons of observed positions and hyperfine patterns with predictions. Because of the difficulty in maintaining constant experimental conditions, extensive signal averaging was not done and many measurements were taken directly from survey scans. Some features which were measured in the discharge showed deviations from calculated positions of 200–300 kHz which could be attributed to their very strong Stark effect. Such transitions were not fitted. However, smaller Stark shifts may have gone unnoticed. As a result, the uncertainties assigned to even the best features were 70 kHz and no $2\nu_2$ features were assigned uncertainties of better than 100 kHz. A few weak features, some of which are from paramagnetic species, remain unassigned. However, large deviations from thermal population were not observed as they were for IO in the same experiment, and highly excited OIO states were not sufficiently populated to be assignable.

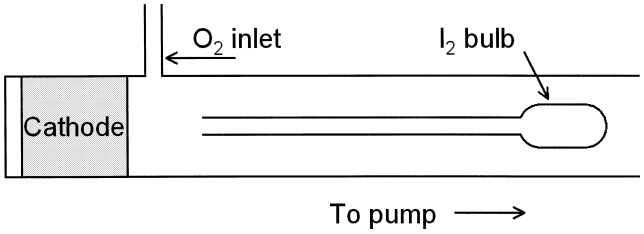

FIG. 2. A schematic top view of the cathode region of the discharge cell. The gases are pumped out at the opposite end of the cell through a sidearm and metal bellows valve which serves as the grounded anode. The drawing is approximately to scale with the bulb neck being 22.9 cm long. The cooling jacket and Zeeman coil surrounding the cell are not shown.

RESULTS

The spectrum and assignment

OIO is a prolate asymmetric rotor ($\kappa=-0.695\,86$) with C_{2v} symmetry about the b axis and a $^2B_1$ electronic ground state. The oxygen spin statistics allow only rotational levels with K_a+K_c odd in the ground and other totally symmetric vibrational states. The rotational, electron spin, and nuclear spin angular momenta are coupled in the following way:

$$N+S=J,$$

$$J+I=F.$$

Therefore, each rotational level has fine structure doubling due to the electron spin and further splitting into sextets by the spin 5/2 iodine nucleus. In the frequency regions searched, only the $\Delta F=\Delta J=\Delta N$ transitions were expected to be observable giving rise to doublets of sextets. Spectra were predicted using fine and hyperfine constants from the ESR work of Byberg.[12,13] The rotational constants were initially calculated using structural parameters estimated from those of related molecules. These calculations indicated that the C rotational constant was about 5.2 GHz. $N+1\leftarrow N$ transitions with a constant value of $N-K_c$ have characteristic spacings of $\approx 2C$ for high N and $K_c\approx N$. These transitions were also predicted to have fine structure doubling of less that 200 MHz and hyperfine splittings of the order of several MHz to several tens of MHz which were not strong functions of N. Thus, it was expected that a survey of ≈11 GHz would reveal at least one recurring pattern. Fortuitously, the transitions with $K_c=N=J+1/2$ have all six strong hyperfine components within 2 MHz. These are only partially resolved from each other and give the appearance of a strong asymmetric doublet with the stronger component at high frequency. Because of the blended lines, these are by far the strongest features in the spectrum. The first of these discovered were the $40_{1,40}\,39.5, F\leftarrow 39_{0,39}\,, 38.5, F-1$ transitions near 420.527 GHz. The recurring pattern was quickly confirmed by skipping to the frequency region of next lower N and conducting a short search. Further confirmation was then obtained from the positions of previously unassigned features contained in survey scans at other frequencies taken during the recently reported IO study.[22] A small region of the OIO spectrum near 420.5 GHz is shown in Fig. 3 under

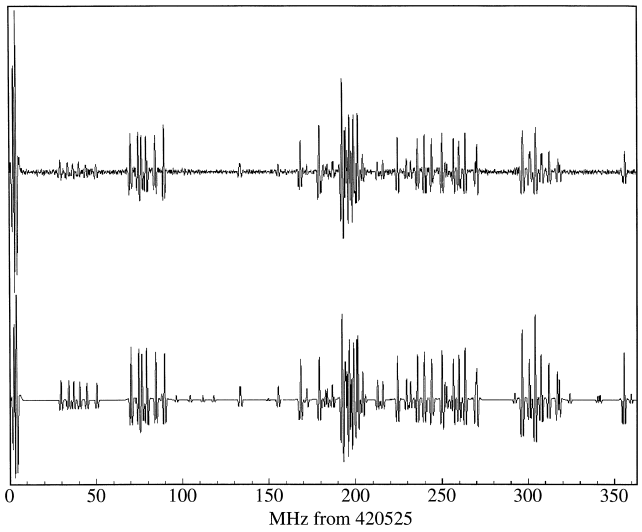

FIG. 3. A portion of the OIO spectrum near 420 525 MHz (top) and a simulation using calculated line positions (bottom). The relative strengths are not reproduced due to power fluctuations of the millimeter wave source and the presence of an electric discharge in the sample. The spectrum was recorded using second harmonic detection. The baseline has been removed from the observed spectrum by taking the second difference using ≈0.5 MHz between points.

nearly optimum conditions. Eventually it was possible to include in the fit a total of 621 ground-state features containing 703 transitions, 198 $v_2=1$ features containing 219 transitions and 72 $v_2=2$ features containing 83 transitions. Several additional features were well described by predictions based on the analysis, but contained blends of different vibrational states and were not included in the fit.

Analysis

The OIO Hamiltonian can be written as

$$H=H_{\mathrm{rot}}+H_{\mathrm{fs}}+H_{\mathrm{hfs}},$$

TABLE I. OIO rotational parameters/MHz.

Parameter[a]	X_{000}	$X_{010}-X_{000}$	$X_{020}+X_{000}-2X_{010}$
A	18 485.940 8(33)	274.876 8(125)	9.424(98)
B	7256.678 87(170)	−2.494 5(72)	−0.130(33)
C	5196.524 42(131)	−10.003 28(98)	−0.016 27(286)
$D_J\times10^3$	6.508 17(123)	−0.037 0(32)	
$D_{JN}\times10^3$	−53.328 2(58)	−1.3573(227)	−0.139(76)
$D_N\times10^3$	307.322 2(266)	23.994(93)	−2.226(251)
$d_1\times10^3$	−2.748 81(79)	−0.008 95(232)	
$d_2\times10^3$	−0.112 748(132)	−0.027 09(60)	
$H_N\times10^6$	0.022 52(38)	0.000 55(42)	
$H_{NK}\times10^6$	−0.308 43(90)	−0.022 6(88)	
$H_{KN}\times10^6$	−2.132 4(244)	−0.046(42)	
$H_K\times10^6$	16.747(128)	2.98(40)	
$h_1\times10^9$	9.99(43)	0.215(225)	
$h_2\times10^9$	0.139(63)	−0.031(69)	
$h_3\times10^9$	1.079 5(68)	0.197(63)	
$L_{KKN}\times10^9$	0.547(43)		
$L_K\times10^9$	−2.179(219)		
$l_1\times10^{12}$	0.110(71)		

[a]The numbers in parentheses are $\sim1\sigma$ uncertainties in units of the last digit.

TABLE II. OIO fine structure parameters/MHz.

Parameter[a]	X_{000}	$X_{010}-X_{000}$	$X_{020}+X_{000}-2X_{010}$
ϵ_{aa}	−2545.472(71)	64.715(171)	8.52(243)
ϵ_{bb}	−620.0597(291)	6.507(116)	−0.320(300)
ϵ_{cc}	197.8051(135)	1.7414(221)	0.101(68)
$D_N^S\times10^3$	−1.8575(70)		
$D_{KN}^S\times10^3$	9.365(123)	0.972(264)	
$D_{NK}^S\times10^3$	0.023(91)		
$D_K^S\times10^3$	−49.12(42)	−13.65(68)	
$d_1^S\times10^3$	−1.2421(36)		
$d_2^S\times10^3$	−0.24584(144)		
$H_{KKN}^S\times10^6$	−0.821(215)		
$H_K^S\times10^6$	4.88(77)		

[a]The numbers in parentheses are $\sim1\sigma$ uncertainties in units of the last digit.

where H_{rot} is a Watson S reduction of the rotational Hamiltonian in the I^r representation[24] which contains up to octic centrifugal distortion terms; H_{fs} is a fine structure Hamiltonian describing the electron spin–rotation with up to sextic distortion terms; and H_{hfs} is a hyperfine structure Hamiltonian which includes spin–spin coupling with quartic distortion terms, and nuclear quadrupole and nuclear spin–rotation coupling. The centrifugal distortion terms for H_{fs} are based on the work of Brown and Sears.[25] All terms in the Hamiltonian are defined in Ref. 21. Although the Hamiltonian is similar to the one used for OBrO,[21] the smaller number of less precisely measured spectral features do not allow the determination of quite as many parameters as were reported for OBrO. Nevertheless, the parameters for the OIO ground and $v_2=1$ states that are to be used to derive the structure and other molecular properties are well determined. The parameters required to fit the spectrum for H_{rot}, H_{fs}, and H_{hfs}, are listed in Tables I–III, respectively. An output file containing correlation coefficients as well as a complete list of fitted lines, estimated experimental uncertainties, and calculated positions is available from the Electronic Physics Auxiliary Publication Service (EPAPS) of the American Institute of Physics.[26] Also available are input files which can be used with the program SPFIT[27] to generate the calculation reported here.

TABLE III. OIO hyperfine parameters/MHz.

Parameter[a]	X_{000}	$X_{010}-X_{000}$
a_F	−90.068(59)	0.321(141)
T_{aa}	−487.117(208)	−0.57(34)
T_{bb}	−564.153(128)	0.35(38)
T_{cc}	1051.270(140)	0.22(37)
$T_{aa}^K\times10^3$	2.03(48)	
$T_{aa}^J\times10^3$	−0.734(147)	
$T_-^K\times10^{3b}$	−45.2(44)	
χ_{aa}	−940.00(47)	−2.68(164)
χ_{bb}	−109.84(45)	−0.51(158)
χ_{cc}	1049.84(48)	3.19(175)
$\chi_-^K\times10^{3b}$	−82.4(173)	
$C_{aa}\times10^3$	138.47(314)	
$C_{bb}\times10^3$	56.70(273)	
$C_{cc}\times10^3$	34.41(204)	

[a]The numbers in parentheses are $\sim1\sigma$ uncertainties in units of the last digit.
[b]$T_-^K=T_{bb}^K-T_{cc}^K$, $\chi_-^K=\chi_{bb}^K-\chi_{cc}^K$.

TABLE IV. Halogen dioxide structures.

	$O^{35}ClO$			$O^{79}BrO$			OIO		
Parameter[a]	r_0	r_e	δr_e	r_0	r_e	δr_e	r_0	r_e	δr_e
r/pm	147.5	147.0	9.9	164.9	164.4	7.3	180.5	(180.0)	6.8
α/deg	117.5	117.4		114.4	114.3		109.9	(109.8)	

[a]The r_0's are calculated from the planar moments. The r_e's are experimental for OClO (Ref. 20), calculated from the r_z and the Kuchitsu (Ref. 28) relationship for OBrO (Ref. 21), and estimated for OIO. The δr_e's are the decreases in bond lengths from the $X_1\,^2\Pi_{3/2}$ states of the corresponding monoxides.

DISCUSSION

Structural parameters

The OIO ground-state effective structure, r_0 can be calculated from any two of the three moments of inertia or the *a* and *b* planar moments. The latter is given in Table IV. The uncertainties of the rotational constants are very small, however, the accuracy of the r_0 structural parameters is limited by vibrational effects which lead to different values depending on the choice of moments. Thus, the uncertainty of each of the r_0 parameters is approximately two units in the last figure quoted. Table IV also compares the r_0 structure with those of OClO and OBrO. For the latter two molecules, the equilibrium structures give bond lengths of 0.5 pm shorter and bond angles 0.1° smaller than the r_0 structures when the planar moments are use for the calculation.[21] Similar differences may be expected for OIO. Since considerably less data exist for the determination of the harmonic force field than were available for OBrO, the more rigorous determination of r_z and r_e structures that was done for OBrO has not been done for OIO. The trend toward smaller bond angle is apparent in going from Cl to I as is shown in Table IV. Also shown for comparison are the decreases of the equilibrium bond lengths from those of the $X_1\,^2\Pi_{3/2}$ states of the corresponding monoxides. It can be seen that the shortening of the bond is only slightly smaller for OIO and than for OBrO and that both are significantly less than is found for OClO. This is to be expected if the π bonding is less effective between atoms of disparate size. *Ab initio* calculations of the structural parameters for OIO and IO by Misra and Marshall[16] give 181.1 pm and 111.4° for the equilibrium bond length and angle in OIO and 188.8 pm for the bond length in IO. The calculated difference in bond length between IO and OIO is very close to that observed, but both the bond length and OIO angle are larger than the experimentally determined values by 1.1 pm and $\approx$1.5°, respectively.

The centrifugal distortion constants are consistent with those of OClO and OBrO. These can be used along with the measured vibrational frequencies[15] for ν_1 and ν_3 and the inertial defects for the ground and excited bending state to roughly determine the harmonic force field. In the fit with the program NCA,[29] the vibrational frequencies are weighted ten times greater relative to their magnitude than are the centrifugal distortion constants and inertial defects. Because the bending mode frequency, ν_2, is not well determined, with values of 192(35) and 250 cm^{-1} having been reported,[3,4] it is not included in the determination of the harmonic force field. The force constants and the observed and calculated molecular constants are shown in Table V. For comparison, the results of a calculation done for OBrO utilizing only data and weighting corresponding to those used for OIO are also shown. The value calculated for the bending frequency of OBrO as well as the values for the diagonal force constants are not significantly different from those derived from the more extensive data used in Ref. 21. The calculated values of f_{rr} and $f_{r\alpha}$ for OBrO change from -5.0 and -6.1 Nm^{-1} in Ref. 21 to 0.4 and -6.8 Nm^{-1} for the more limited data set used here. Thus even with the smaller data set it is apparent that changes in the constants f_r and f_α on replacing Br with I are much less than those when Cl is replaced by Br. This is consistent with the observation that the O–X bond length changes are relatively less for both the Br and I on going from the monoxide to the dioxide and that double bond formation is less effective in both heavier dioxides.

The harmonic force field calculation predicts the ν_2 frequency to be 263 cm^{-1}, which is only 13 cm^{-1} higher than the estimate of Himmelmann *et al.*[4] The corresponding calculation of for OBrO gives a result that is $\approx$4 cm^{-1} lower than the observed frequency. This is not necessarily predictive of the difference between the OIO calculated and actual ν_2. However, the present result certainly favors the estimate of $\approx$250 cm^{-1} from the study of the ultraviolet (UV) spectrum[4] over the much lower value obtained from photoelectron detachment. Moreover, Hullah and Brown[30] recently

TABLE V. Comparison of harmonic force field calculations for OIO and OBrO using similar data sets and weighting.

	OIO		$O^{79}BrO$	
Parameter	Obs.	Calc.	Obs.	Calc.
ω_1/cm^{-1}	768.0[a]	768.1	811.6	812.0
ω_2/cm^{-1}	250.0[c]	263.0	320.0	315.9
ω_3/cm^{-1}	800.3[a]	800.3	865.6	865.3
D_J/kHz	6.508	6.667	7.135	7.169
D_{JK}/kHz	−53.32	−53.29	−70.69	−70.70
D_K/kHz	307.3	296.2	714.4	694.7
d_1/kHz	−2.749	−2.799	−2.638	−2.647
d_2/kHz	−0.1127	−0.1051	−0.1568	−0.1395
Δ_{000}/amuÅ^2	0.2717	0.2736	0.2278	0.2297
Δ_{010}/amuÅ^2	0.8359	0.8340	0.7032	0.7025
f_r/Nm^{-1}		511.9		548.9
f_α/Nm^{-1}		93.3		102.4
f_{rr}/Nm^{-1}		−4.5		0.4
$f_{r\alpha}$/Nm^{-1}		−15.6		−6.8

[a]From Ref. 15.
[b]Not included in the fit for either molecule.
[c]From Ref. 4.

TABLE VI. Normalized electron spin–rotation coupling constants, electronic g values, and ratios of Λ_{ii}^e for OXO.

	OIO		$O^{79}BrO$		$O^{35}ClO$		I–Br	Br–Cl
i	$-\Lambda_{ii}^e/2$[a]	g_{ii}'[a]	$-\Lambda_{ii}^e/2$	g_{ii}'	$-\Lambda_{ii}^e/2$	g_{ii}'	Λ_{ii}^e	Λ_{ii}^e
a	0.0688	0.0881	0.0420	0.0512	0.0133	0.0133	1.6404	3.1486
b	0.0427	0.0279	0.0344	0.0302	0.0109	0.0109	1.2438	3.1513
c	−0.0190	−0.0324	−0.0041	−0.0620	−0.0003	−0.0003	4.6032	15.17

[a]Gas phase; $\Lambda_{ii}^e=\epsilon_{ii}/B_i$. Matrix ESR; $g_{ii}'=g_{ii}-g_e$.

studied the TeO_2 electronic spectrum and found $\nu_2=282$ cm^{-1}. The value of ν_2 in OBrO is 45 cm^{-1} less than in SeO_2, and this may be taken as an upper limit for the difference between the ν_2 values of OIO and TeO_2. Thus, the features attributed to ν_2 hot bands in the OIO UV spectrum reported by Himmelmann *et al.*[4] are probably correctly assigned.

Electron spin–rotation coupling constants

Table II shows the electron spin–rotation constants, their centrifugal distortion constants, and their dependence on the ν_2 excitation. In Table VI the normalized spin–rotation constants, $\Lambda_{ii}^e=\epsilon_{ii}/B_i$, are compared with those of OBrO and OClO as well as the g values, $g_{ii}'=g_{ii}-g_e$ determined by ESR spectroscopy of matrix isolated molecules. The relationship proposed by Curl[31] between the normalized electron spin–rotation constants and the electronic g values obtained from ESR experiments

$$-\Lambda_{ii}^e/2=g_{ii}-g_e,$$

where g_e is the free electron, g factor predicts the trends observed for the g values in matrix isolated samples.[12,32] Possible structural perturbations in the matrix prevent detailed interpretation of the differences between observed and calculated values for the heavier halogen dioxides.

The normalized spin–rotation constants increase from OClO to OIO, but the increase from OBrO to OIO is neither as large nor as uniform as would be estimated from the increase from OClO to OBrO. In the latter case, both Λ_{aa}^e and Λ_{bb}^e increase by an amount which is very close to the spin–density weighted average of the atomic spin–orbit coupling constants and by a slightly larger factor than for the ratio of spin–orbit coupling constants in the monoxides. For OIO the corresponding estimated change would be more than an additional factor of 2 increase compared to OBrO as is seen in the spin–orbit coupling of IO.[3] However, Λ_{aa}^e increases by an additional factor of only 1.64 and Λ_{bb}^e by a factor of only 1.24. Since the excitation energies are smaller for OIO than for the lighter dioxides, this is an indication that the matrix elements connecting the ground state with the perturbing states are smaller than would be estimated by considering only p orbital spin–orbit couplings. The increase in magnitude of Λ_{cc}^e is very large and may indicate increased participation of d orbitals in the excited states that contribute to the electron spin–rotation constants or contributions from states requiring excitation of more than one electron. Curl[33] has discussed this topic for the case of OClO.

A complete set of quartic and some sextic spin–rotation distortion terms are required to fit the ground rotational state spectrum. The trends observed for OBrO and OClO are continued for OIO in the sense that trends to more positive or more negative values are maintained for the quartic constants. The values are actually quite different among the three molecules and are compared in Table VII. Less data are available for the excited bending states than for the lighter dioxides and only two independent quartic distortion terms could be determined for the ν_2 state.

The changes in spin–rotation constant with bending mode excitation follow the trend shown in OClO and OBrO. This is shown in Table VIII where the changes with excitation of Λ_{ii}^e, B_i, and ϵ_{ii} divided by their ground state values are given. The values of $|\epsilon_{aa}|$ decrease by a relatively greater amount for the heavier halogens whereas the change in $|\epsilon_{bb}|$ starts as positive for OClO, becomes negative for OBrO and more strongly negative for OIO. Although $|\epsilon_{cc}|$ is more than a factor of 10 larger for OBrO than it is for OClO and increases by almost another factor of 4 for OIO the relative

TABLE VII. Comparison of the OXO electron spin–rotation constants and quartic distortion terms/MHz.

Parameter	OIO	$O^{79}BrO$	$O^{35}ClO$
ϵ_{aa}	−2545.472(71)	−2352.2192(157)	−1388.2793(126)
ϵ_{bb}	−620.0597(291)	−565.6644(56)	−216.9293(58)
ϵ_{cc}	197.8051(135)	52.5741(60)	4.6022(54)
$D_N^S\times10^3$	−1.8575(70)	−0.372 46(269)	−0.1228(58)
$D_{NK}^S\times10^3$	0.023(91)	−0.6245(275)	−1.529(115)
$D_{KN}^S\times10^3$	9.365(123)	−0.305(34)	−3.454(140)
$D_K^S\times10^3$	−49.12(42)	−17.205(191)	−0.683(151)
$d_1^S\times10^3$	−1.2421(36)	−0.343 27(204)	−0.093 66(67)
$d_2^S\times10^3$	−0.245 84(144)	−0.115 08(108)	−0.022 88(37)

TABLE VIII. Changes of the normalized electron spin–rotation constants, rotational constants, and electron spin–rotation constants for OXO with excitation of ν_2. The tabulated quantities are $100(X_{010}-X_{000})/X_{000}$.

	OIO			$O^{79}BrO$			$O^{35}ClO$		
i	Λ_{ii}^e	B_i	ϵ_{ii}	Λ_{ii}^e	B_i	ϵ_{ii}	Λ_{ii}^e	B_i	ϵ_{ii}
a	−3.97	1.49	−2.54	−3.63	1.76	−1.94	−2.79	1.92	−0.92
b	−1.01	−0.03	−1.05	−0.18	−0.06	−0.24	0.27	−0.09	0.18
c	1.07	−0.19	0.88	1.19	−0.25	0.94	1.31	−0.29	1.02

changes with excitation actually decrease slightly for the heavier molecules.

Spin–spin coupling constants

The spin–spin coupling constants for both the ground and ν_2 states have been determined as have some centrifugal distortion constants common to both states. The available $2\nu_2$ data have been adequately fit by assuming linear changes with excitation of the bending mode for all of the hyperfine constants shown in Table III. The anisotropic or dipolar coupling tensor, **T**, and scalar or Fermi contact term, a_F, are well determined and consistent with the trends observed for OClO and OBrO. The signs and magnitudes of the centrifugal and vibrational terms are also consistent with those of OBrO and OClO, but are less precisely determined than the OBrO constants. Of interest is the negative a_F value of $-90.07(6)$ MHz which can be compared to the $-95.8(3.8)$ MHz Fermi contact term of IO.[22] Byberg[12,13] obtained a similar result in his study of the OIO ESR spectrum and pointed out that a negative value of about this magnitude is predicted from the calculated relativistic atomic value for an iodine $5p$ electron[34] and the spin density on the iodine. For a spin density of ~0.5 on the I atom, one predicts $a_F \approx -115$ MHz. The contact term for a single $5s$ electron in atomic iodine is 46.6 GHz.[35] Therefore, as was also found for OClO and OBrO, there must be almost no halogen s character in the orbital containing the unpaired electron.

The dipolar coupling tensor is very nearly axially symmetric about an axis parallel to the c principal axis of the molecule. The components of the tensor are given by

$$T_{xx}=g_e g_N \mu_e \mu_N \langle (3\cos^2\ \theta_x - 1)/r^3 \rangle_S ,$$

where x is one of the principal axes of the molecule and $\cos\theta_x$ is the direction cosine of the vector from the nuclear spin to the electron spin. It is usually assumed that the spin density at the halogen in the OXO molecules is primarily due to a p electron in an orbital perpendicular to the molecular plane with the atomic angular distribution given by $\langle 3\cos^2\theta_x - 1\rangle = 0.8, -0.4, -0.4$ for $x=c,a,b$, respectively. For the present case, T_{aa} is slightly less negative than T_{bb} so that $\langle\cos^2\theta_a\rangle > \langle\cos^2\theta_b\rangle$. For OClO, OBrO, and OIO the asymmetry parameter

$$\eta_T=(T_{aa}-T_{bb})/T_{cc},$$

has values of 0.033 82, 0.044 65, 0.073 28, respectively. A similar trend toward increasing asymmetry is seen in the series NH_2, PH_2, and AsH_2[36–39] although in the case of the group V dihydrides the unpaired electron is in a $p\pi$ bonding orbital with the spin density almost entirely on the central atom. In the halogen dioxides the unpaired electron is in an antibonding orbital with about half the spin density on the central atom. This slight axial asymmetry of the dipolar coupling tensor may be thought of as a contribution from a small amount of in-plane electron spin density due to mixing of the $X\,^2B_1$ state with excited electronic states of A_1 and B_2 symmetry, primarily by off-diagonal elements of the spin–orbit coupling. Peterson[40] has recently performed *ab initio* calculations for OClO and OBrO. Using the same level of theory described in Ref. 40, he has calculated small (1%) in-plane spin densities for both OClO and OBrO oriented oppositely to that in the p_c orbital with most of the in-plane spin density along the symmetry axis.[41] While such small calculated values are to be treated cautiously, they are the magnitude and sign indicated by the observed asymmetry of the dipolar coupling tensor.

As mentioned in the discussion of the spin–rotation constants, the ϵ_{ii}'s of OIO do not closely follow the trend expected for similar halogen spin densities for the three dioxides. However, the ϵ_{ii}'s are described primarily by the interaction of the ground state with various excited electronic states whereas the spin–spin interactions as well as the quadrupole coupling constants discussed below are primarily described by the ground-state wave function.

For the halogen monoxides, the spin density can be derived directly from the Frosch–Foley[42] constants

$$d + c/3 = \rho_S(\mathrm{XO}) g_e g_N \mu_e \mu_N \langle r^{-3}\rangle_S(\mathrm{atom}),$$

where the S subscript refers to the appropriate expectation value for the radial distribution of the electron spin. For the dioxides the angular dependence cannot be removed. If one ignores the small amount of in-plane spin density, the approximate spin density for a $p\pi$ orbital may be derived from a similar expression with $5T_{cc}/4$ replacing $d+c/3$ on the left-hand-side of the above equation. Thus, one obtains

$$\rho_S(\mathrm{OXO})/\rho_S(\mathrm{XO}) \approx (5T_{cc}/4)/(d+c/3).$$

This ratio equals 1.42, 1.38, and 1.33 for the Cl,[20,43] Br,[21,44] and I[22] compounds, respectively. This shows that the shift in spin density to the more electropositive element is less pronounced in the dioxides than in the monoxides.

A single electron in the valence p_c orbital would result in T_{cc} values of 2068.3, 1569.3, and 295.4 MHz for I, ^{79}Br, and ^{35}Cl, respectively. The T_{cc}'s are determined by using the relativistic values calculated by Pyykkö and Wiesenfeld[35] to obtain the $\langle r^{-3}\rangle_S$'s for the atoms. The hyperfine integrals from Table A2 of Ref. 35 are related to the r_{++}, r_{+-}, and r_{--} terms from Ref. 34: $V(1)=2r_{--}$, $V(1,-2)=r_{+-}/2$ and $V(-2)=-r_{++}$. The atomic iodine radial expectation

values are then determined from the relationships $\langle r^{-3}\rangle_L = (4r_{++}+4r_{--}+r_{+-})/9$ and $\langle r^{-3}\rangle_S = (-8r_{++}+40r_{--}-5r_{+-})/27$. Where the L and S subscripts refer to orbital and spin distributions. The numerical results require a factor of $a_0^{-3}\alpha^{-1}$ to convert them into SI units. These values of T_{cc} lead to halogen spin densities of 0.508, 0.498, and 0.544 for OIO, OBrO, and OClO respectively. The experimental magnetic constants for ^{35}Cl atom reported by Uslu *et al.*[45] would give a T_{cc} of 330.7 MHz and result in a Cl spin density of 0.486 for OClO.

Note that the effect of the positive charge on the halogen has not been considered when using the atomic value of $\langle r^{-3}\rangle_S$ for either the monoxides or the dioxides. In fact, the halogens are positively charged in both compounds and it may be more appropriate to apply a correction factor to account for the nucleus being less shielded from the valence electrons. For all the halogen nuclei a factor of $1+0.15n_e$ is used for quadrupole coupling,[46] where n_e is the charge on the atom. If we assume that this is primarily due to a change in $\langle r^{-3}\rangle_T$ for all the electrons, then a similar factor may be applicable to $\langle r^{-3}\rangle_S$. In that case the spin density on the halogens would be less than that given above, or about 0.4 for all three dioxides. The details of the calculation which takes charge into consideration are discussed in the section on quadrupole coupling.

Recent studies of the halogen monoxides have shown that the angular distribution of the electron about the halogen atom in those molecules changes from slightly elongated to slightly compressed with respect to the atomic p orbital as the atomic number increases.[22] For the dioxides it is apparent from the slight asymmetry of the coupling tensor about the c axis that there is at least some difference in the angular distribution of the spin density about the halogen from that of a pure p_c-orbital and that the difference increases with atomic number. The uncertainty regarding the angular distribution of the spin density as well as the uncertainty of the theoretical radial functions limit the accuracy of the spin density derived from the spin–spin coupling tensor. Should the angular distribution of the electron change in a manner similar to that observed for the monoxides, then the spin density of I would be greater, and that of Cl less than that given by the calculation described in the preceding paragraph. However, Byberg's ESR study[13] of ^{17}O enriched OIO and OClO showed little change in spin density at the oxygen. That result was consistent with his earlier studies of the ^{16}O compounds[12] which showed similar spin densities at the halogens in each of the dioxides. This suggests that the angular distribution of the electron spin about the halogen is quite well described by that of an atomic p-electron and is about the same for all three OXO dioxides. The fact that the effect of the double bond on bond length and strength is much less in OBrO and OIO than it is in OClO may not be an important consideration, since the electron distribution closest to the coupling nucleus is most significant in the determination of the dipolar coupling tensor.

Nuclear quadrupole coupling constants

The quadrupole coupling constants are consistent with those of OBrO and OClO. These may be interpreted in terms of the in-plane p electron population if the out of plane population is fixed to that derived from the spin–spin coupling tensor. Because the π and π^* orbitals are orthogonal, the total $p\pi$ electron density at the I atom is given by $2-\rho_c^s$ where ρ_c^s is the spin density determined from T_{cc}. One then obtains the total in-plane p electron density at the I atom from

$$\rho_a^t+\rho_b^t = 2(2-\rho_c^s-\chi_{cc}/eQq_{510}^{\mathrm{eff}}).$$

The ρ_x^t are the total electron densities in the p_a and p_b orbitals. The individual densities may be determined from

$$\rho_a^t-\rho_b^t = 2(\chi_{aa}-\chi_{bb})/(3eQq_{510}^{\mathrm{eff}}).$$

The effective atomic quadrupole coupling constants are corrected for the positive charge on the halogen which requires information on the participation of s and d orbitals in the bonds. Peterson[41] has found little contribution from d orbitals in both OClO and OBrO and the same will be assumed true for OIO. If one describes the in-plane orbitals in terms of the usual sp^n hybridization, then

$$\psi_1 = (1-2a_s^2)^{1/2}\psi_s + 2^{1/2}a_s\psi_{pb},$$

$$\psi_2 = a_s\psi_s - (1/2-a_s^2)^{1/2}\psi_{pb} + 2^{-1/2}\psi_{pa},$$

$$\psi_3 = a_s\psi_s - (1/2-a_s^2)^{1/2}\psi_{pb} - 2^{-1/2}\psi_{pa},$$

where $a_s^2 = \cos\alpha/(\cos\alpha-1)$ and $\alpha = \angle\mathrm{OXO}$.[47] Since the electron density in each of the two orbitals in the oxygen directions must equal ρ_a, one has

$$\rho_l = (\rho_b-\rho_a(1-2a_s^2))/2a_s^2,$$

$$\rho_s = (1-2a_s^2)\rho_l + 2a_s^2\rho_a,$$

$$n_e = 7-(\rho_a+\rho_b+\rho_c+\rho_s),$$

where ρ_l is the population of the lone pair orbital described by ψ_1 and ρ_s is the total s orbital population. These equations may be solved for ρ_l, ρ_s, and n_e with a_s fixed by the bond angle or for a_s and the remaining parameters with ρ_l fixed. Since ρ_a, ρ_b, and ρ_c depend on n_e due to the multiplicative factor of $1+0.15n_e$ applied to the atomic quadrupole and magnetic coupling constants, the equations must be solved iteratively.

If one uses α's fixed to the values obtained from the r_0 structures, eQq_{n10}^{eff} corrected for relativistic effects as discussed by Pyykkö and Seth,[48] and ρ_c^s determined from T_{cc}, then one obtains the p orbital electron populations given in Table IX. For I, ^{79}Br, and ^{35}Cl, the respective relativistic correction factors and resultant values of eQq_{n10}^{eff} for the neutral atoms are 1.0912, 1.0356, and 1.0075 giving 2501.83, −797.18, and 110.568 MHz. For OClO the calculation was done with both atomic T_{cc} values mentioned in the preceding section. This calculation gives similar in-plane p electron densities for all of the halogens and does not show the expected trend to lower electron density on the more electropositive element. If the amount of s character in the halogen σ bonding orbitals were determined solely by the OXO angle, then it would be necessary to remove about 0.5 electron from the ''lone pair'' orbital for all of the halogens in order to reproduce the observed quadrupole couplings. With

TABLE IX. Orbital populations and related parameters derived from the hyperfine constants.

	Fixed hybridization[a]				Full lone pair[b]			
	OIO	OBrO	OClO	OClO[c]	OIO	OBrO	OClO	OClO[c]
ρ_a	1.161	1.112	1.086	1.117	1.120	1.067	1.041	1.077
ρ_b	1.339	1.335	1.348	1.383	1.307	1.302	1.316	1.355
ρ_c	1.589	1.602	1.569	1.609	1.569	1.582	1.548	1.591
ρ_c^s	0.411	0.398	0.431	0.391	0.431	0.418	0.452	0.409
ρ_s	1.333	1.271	1.238	1.272	1.812	1.766	1.725	1.721
ρ_l	1.513	1.494	1.500	1.538	2.000	2.000	2.000	2.000
a_s^2	0.254	0.292	0.316	0.316	0.106	0.126	0.143	0.151
α	109.9	114.4	117.5	117.5	96.8	98.3	99.6	100.2
n_e	1.577	1.681	1.759	1.619	1.192	1.283	1.256	1.369

[a]The s character given by a_s^2 is determined by the r_0 bond angle α shown here in degrees.
[b]The lone pair orbital population, ρ_l, is fixed at 2. The s character and resultant angle are calculated.
[c]Calculated using T_{cc} for a single electron derived from the atomic constants determined by Uslu *et al.* (Ref. 45).

the lone pair orbital on the halogen fully occupied, Table IX shows that the required values of a_s^2 and the corresponding bond angles are considerably less than those determined from the positions of the nuclei. The calculated angles decrease as do the experimental angles, but all are much smaller. The orbital populations given in Table IX show that the main difference in the two calculations is that the latter keeps the lone pair in an orbital that is largely s character. The seemingly anomalous result that the I atom is less positive than Br or Cl is common to both calculations and may indicate a more important role for d orbitals in I or that the simple model used here is not capable of showing subtle trends. It is clear, however, that there is little change in the valence electron distribution closest to the central atom in spite of significant changes in bond angle. Although the experimentally determined and theoretically calculated values of T_{cc} for Cl atom produce somewhat different derived electron distributions, these differences do not affect the above conclusions.

It is interesting that the *ab initio* calculations of Peterson[40,41] at the B3LYP/aug-cc-pVDZ level of theory give about 13% s character for the halogen σ bonding orbitals on OClO and OBrO with little d character. This may be compared with the 14.3% or 15.1% OClO and 12.6% OBrO s character shown in Table IX. Thus, both theory and the quadrupole coupling constants indicate considerably less s character than the bond angle would indicate. Peterson's calculations also show that for OClO and OBrO the electron distributions at the halogens are almost the same. Experiment supports this and extends the similarity to OIO. In addition to the Peterson calculations there have recently been *ab initio* calculations for OClO which have yielded hyperfine constants[49] in good agreement with experiment. The hyperfine constants reported in this study should be useful in testing the quality of such calculations for OIO.

Nuclear spin–rotation constants

The nuclear spin–rotation coupling constants have been well determined for OIO and are compared with those of OBrO and OClO in Table X along with the normalized constants given by

$$\Lambda_{ii}^n = C_{ii}/(B_i g_n \langle r^{-3}\rangle_l),$$

where g_n is the nuclear g factor. The trend toward larger values of Λ_{ii}^n is as expected for molecules with lower lying excited electronic states. Unlike $\mathbf{\Lambda}^e$, $\mathbf{\Lambda}^n$ is nearly isotropic for all three halogen dioxides. It is interesting that the halogen monoxides all have normalized nuclear spin–rotation coupling constants very close to those of the OXO dioxides. These are 5.5, 4.3, and 3.5×10^{-38} m^3 for IO, BrO, and ClO, respectively.

CONCLUSION

This investigation of the rotational spectrum of OIO has completed the series of studies of the known OXO halogen dioxides. An extensive set of molecular parameters has been determined which can provide accurate predictions of the rotational spectra of the ground and first excited bending state and will be helpful in the analysis of any rotationally resolved OIO spectra. It has been possible to elucidate trends in structure and harmonic force field for the Cl, Br, I series. The force field calculation has provided confirmation for the determination of the bending frequency from the optical spectrum and has shown that there is relatively less difference in bond strength between the IO and BrO bonds than between the BrO and ClO bonds. The values of Λ_{aa}^e and Λ_{bb}^e are somewhat smaller than expected based on the estimated spin–orbit coupling for the molecule and the corresponding values for OClO and OBrO. The hyperfine parameters are in good agreement with ESR results[12,13] indicating only minor matrix effects in the earlier study. Both the magnetic and

TABLE X. Nuclear spin–rotation coupling constants, for OIO, OBrO, and OClO.

	OIO		OBrO		OClO	
i	C_{ii}/kHz	Λ_{ii}^n[a]	C_{ii}/kHz	Λ_{ii}^n[a]	C_{ii}/kHz	Λ_{ii}^n[a]
a	138.5(31)	5.4(1)	160.1(27)	4.7(1)	45.5(33)	3.5(3)
b	56.7(27)	5.7(4)	41.6(17)	4.2(2)	8.8(10)	3.5(4)
c	34.4(20)	4.8(3)	31.7(18)	4.1(2)	7.9(9)	3.8(4)

[a]$\Lambda_{ii}^n = C_{ii}/(B_i g_n \langle r^{-3}\rangle_l) \times 10^{38}/\mathrm{m}^3$.

quadrupole coupling constants indicate little change in electron distribution at the halogen for the entire series. The hyperfine constants also indicate that there is little difference in the amount of *s* orbital character in the σ bonds and that the *s* character is less than is indicated by the bond angles. It is hoped that the accurate parameters provided by this work will be of use in judging the quality of future *ab initio* calculations.

ACKNOWLEDGMENTS

This paper presents research carried out at the Jet Propulsion Laboratory, California Institute of Technology, under contract with the National Aeronautics and Space Administration.

[1] M. W. Chase, J. Phys. Chem. Ref. Data **25**, 1297 (1996).
[2] M. H. Studier and J. L. Huston, J. Phys. Chem. **71**, 457 (1967).
[3] M. K. Gilles, M. L. Polak, and W. C. Lineberger, J. Chem. Phys. **96**, 8012 (1992).
[4] S. Himmelmann, J. Orphal, H. Bovensmann, A. Richter, A. Ladstätter-Weissenmayer, and J. P. Burrows, Chem. Phys. Lett. **251**, 330 (1996).
[5] R. P. Wayne, G. Poulet, P. Biggs *et al.*, Atmos. Environ. **29**, 2677 (1995); see Sec. III C 9 and references cited.
[6] O. V. Rattigan, R. L. Jones, and R. A. Cox, Chem. Phys. Lett. **230**, 121 (1994).
[7] D. M. Rowley, W. J. Bloss, R. A. Cox, and R. L. Jones, J. Phys. Chem. A **105**, 7855 (2001).
[8] T. Ingham, M. Cameron, and J. N. Crowley, J. Phys. Chem. A **104**, 8001 (2000).
[9] B. J. Allan, J. M. C. Plane, and G. McFiggans, Geophys. Res. Lett. **28**, 1945 (2001).
[10] T. Hoffmann, T. C. D. O'Dowd, and J. H. Seinfeld, Geophys. Res. Lett. **28**, 1949 (2001).
[11] N. M. Atherton, J. R. Morton, K. F. Preston, and S. J. Strach, J. Chem. Phys. **74**, 5521 (1981).
[12] J. R. Byberg, J. Chem. Phys. **85**, 4790 (1986).
[13] J. R. Byberg, J. Chem. Phys. **88**, 2129 (1988).
[14] J. R. Byberg and J. Lindberg, Chem. Phys. Lett. **33**, 612 (1975).
[15] G. Maier and A. Bothur, Chem. Ber.-Recl. **130**, 179 (1997).
[16] A. Misra and P. Marshall, J. Phys. Chem. A **102**, 9056 (1998).
[17] R. F. Curl, Jr., J. L. Kinsey, J. G. Baker, J. C. Baird, G. R. Bird, R. F. Heidelberg, T. M. Sugden, D. R. Jenkins, and C. N. Kenney, Phys. Rev. **121**, 1119 (1961).
[18] M. Tanoura, K. Chiba, K. Tanaka, and T. Tanaka, J. Mol. Spectrosc. **95**, 157 (1982).
[19] K. Miyazaki, M. Tanoura, K. Tanaka, and T. Tanaka, J. Mol. Spectrosc. **116**, 435 (1986).
[20] H. S. P. Müller, G. O. Sørensen, M. Birk, and R. R. Friedl, J. Mol. Spectrosc. **186**, 177 (1997).
[21] H. S. P. Müller, C. E. Miller, and E. A. Cohen, J. Chem. Phys. **107**, 8292 (1997).
[22] C. E. Miller and E. A. Cohen, J. Chem. Phys. **115**, 6459 (2001).
[23] H. M. Pickett, Appl. Opt. **19**, 2745 (1980).
[24] J. K. G. Watson, in *Vibrational Spectra and Structure*, edited by J. R. Durig (Elsevier, Amsterdam, 1977), Vol. 6, p. 189.
[25] J. M. Brown and T. J. Sears, J. Mol. Spectrosc. **75**, 111 (1979).
[26] See EPAPS Document No. JCPSA6-118-002309 for the observed transition frequencies of OIO used in the fit, assignments and residuals as well as input parameter and line files for the program SPFIT. A direct link to this document may be found in the online article's HTML reference section. The document may also be reached via the EPAPS homepage (http://www.aip.org/pubservs/epaps.html) or from ftp.aip.org in the directory /epaps/. See the EPAPS homepage for more information.
[27] H. M. Pickett, J. Mol. Spectrosc. **148**, 371 (1991).
[28] K. Kutchitsu, J. Chem. Phys. **49**, 4456 (1968); K. Kutchitsu, T. Fukuyama, and Y. Morino, J. Mol. Struct. **1**, 463 (1968); **4**, 41 (1969).
[29] D. Christen, J. Mol. Struct. **48**, 101 (1978).
[30] D. F. Hullah and J. M. Brown, J. Mol. Spectrosc. **200**, 261 (2000).
[31] R. F. Curl, Mol. Phys. **9**, 585 (1965).
[32] F. J. Adrian, J. Bohandy, and B. F. Kim, J. Chem. Phys. **85**, 2692 (1986).
[33] R. F. Curl, J. Chem. Phys. **37**, 779 (1962).
[34] I. Lindgren and A. Rosén, Case Stud. At. Phys. **4**, 197 (1974).
[35] P. Pyykkö and L. Wiesenfeld, Mol. Phys. **43**, 557 (1981).
[36] H. S. P. Müller, H. Klein, S. P. Belov, G. Winnewisser, I. Morino, K. M. T. Yamada, and S. Saito, J. Mol. Spectrosc. **195**, 177 (1999).
[37] M. Kajita, Y. Endo, and E. Hirota, J. Mol. Spectrosc. **124**, 66 (1987).
[38] H. Fujiwara, K. Kaori, O. Hiroyuki, and S. Saito, J. Chem. Phys. **109**, 5351 (1998).
[39] R. A. Hughes, J. M. Brown, and K. M. Evenson, J. Mol. Spectrosc. **200**, 210 (2000).
[40] K. A. Peterson, J. Chem. Phys. **109**, 8864 (1998).
[41] K. A. Peterson (private communication).
[42] R. A. Frosch and H. M. Foley, Phys. Rev. **88**, 1337 (1952).
[43] B. J. Drouin, C. E. Miller, E. A. Cohen, G. Wagner, and M. Birk, J. Mol. Spectrosc. **207**, 4 (2001).
[44] B. J. Drouin, C. E. Miller, H. S. P. Müller, and E. A. Cohen, J. Mol. Spectrosc. **205**, 128 (2001).
[45] K. A. Uslu, R. F. Code, and J. S. M. Harvey, Can. J. Phys. **52**, 2135 (1974).
[46] C. H. Townes and A. L. Schawlow, *Microwave Spectroscopy* (McGraw-Hill, New York, 1955).
[47] W. Gordy and R. L. Cook, *Microwave Molecular Spectra, 3rd ed., Techniques of Chemistry, Vol. XVIII* (Wiley-Interscience, New York, 1984).
[48] P. Pyykkö and M. Seth, Theor. Chem. Acc. **96**, 92 (1997).
[49] B. Fernández, O. Christiansen, P. Jørgensen, J. Byberg, J. Gauss, and K. Ruud, J. Chem. Phys. **106**, 1847 (1997).